Top-down fabrication of biodegradable multilayer tunicate cellulose films with controlled mechanical properties

Da Huang
Hubei University
Dong Li
Wuhan University
Kangwei Mo
Wuhan University
Rui Xu
Wuhan University
Yanan Huang
Wuhan University
Yande Cui
Wuhan University
Qunchao Zhang
Hubei University
Chunyu Chang (changcy@whu.edu.cn)
Wuhan University https://orcid.org/0000-0002-3531-5964

Research Article

Keywords: Top-down approach, Tunicate cellulose, Hot pressing, Biodegradability

Posted Date: March 11th, 2021

DOI: https://doi.org/10.21203/rs.3.rs-243240/v1

Abstract

Owing to non-degradable waste plastics caused serious environmental pollution, development of natural polymeric materials has become an important topic. Herein, multilayer tunicate cellulose films (MTCFs) were fabricated by a top-down approach, where the alkali treated mantles of tunicate were layer-by-layer hot-pressed. Strong hydrogen bonds that formed between tunicate cellulose layers resulted in good interfacial compatibility of multilayer films. The as-prepared MTCFs exhibited improved thermal stabilities, excellent mechanical properties, and good degradability in natural soil. This work provided a top-down approach for the preparation of biodegradable multilayer films as packaging materials.

Introduction

Owing to their low cost and high performance, traditional plastics derived from petroleum such as polyethylene (PE), polypropylene (PP), polyvinylchloride (PVC), and polyethylene terephthalate (PET) have been increasingly used as packaging materials (Geyer et al. 2017; Siracusa et al. 2008). However, the tremendous consumption of plastics has led to the production of a large amount of plastic waste, which has triggered global environmental problems (Huang et al. 2020). In the marine environment, the accumulation of plastic debris has become a major global issue which seriously threatened food security, food safety and human health (Barboza et al. 2018). For sustainable development, it is emergency to seek out biodegradable materials to replace petroleum-based plastics (Mohanty et al. 2018). Therefore, natural polymers have been widely concerned for the construction of environmentally friendly materials, due to their abundant, low cost, safe, and biodegradability (Klemm et al. 2005).

Cellulose is the quintessential sustainable resource and the most abundant natural polymer on Earth, which has various applications from energy to materials in the society (Cheng et al. 2016; Peng et al. 2020). Transparent films composed of cellulose nanofibers that formed in aqueous solution exhibited high transparency, mechanical flexibility, high strength, excellent thermal stability, non-toxicity, outstanding printability, and biodegradability (Ye et al. 2019). This bottom-up technique for the construction of cellulose-based materials usually required a complicated preparation process. Recently, a top-down strategy has been employed to create functional cellulose-based materials from wood, which were widely used in building materials, flexible electronics, packaging, and electronics storage devices (Gao et al. 2016; Hu et al. 2018; Jia et al. 2017; Jiang et al. 2018; Jung et al. 2015; Koppolu et al. 2019; Li et al. 2016; Li et al. 2018; Li et al. 2019; Wang et al. 2017; Wang et al. 2018; Zhu et al. 2016a; Zhu et al. 2016b; Zhu et al. 2017; Zhu et al. 2018). For example, isotropic paper obtained from anisotropic wood through a top-down approach with high transmittance and high haze was an excellent substrate for disposable electronic and optical devices (Zhu et al. 2018). In order to develop functional materials, scholars filled the delignified wood with polymers, such as polyvinylpyrrolidone and epoxy resin, so these composite materials had good light management effects and could improve the efficiency of solar cells and serve as energy efficient building materials (Li et al. 2016; Zhu et al. 2016b). However, these wood-derived cellulose materials were obtained by delignification and a multitude of further processing steps, because the tight association of cellulose, hemicellulose, and lignin resulted that lignin could not be

selectively removed from the cell wall of wood by chemical treatment (Keplinger et al. 2020). Unlike wood, tunicate is a kind of sea animal with unique integumentary tissue (tunic) that were composed of crystalline cellulose embedded with protein, lipids, sulfated glycan and mucopolysaccharides (Quero et al. 2018; Zhao and Li 2014). After removal of protein and other components, tunicate cellulose exhibited larger molecular weight, higher crystallinity (I_b), better thermal stability and higher modulus (143 GPa) in comparison with plant cellulose (Cheng et al. 2017; Cheng et al. 2018; Zhan et al. 2018; Zhan et al. 2018). To the best our knowledge, tunicate cellulose films with good mechanical properties prepared from purified tunics are scarcely reported.

Herein, we developed a top-down approach to fabricate transparent tunicate cellulose-based films. Firstly, tunicate cellulose films were obtained by alkaline treatment of the tunics from *Ciona intestinalis*, according to the reported method (Zhao et al. 2018). Secondly, multilayer tunicate cellulose films (MTCFs) were prepared by layer-by-layer hot pressing of above tunicate cellulose films. This top-down strategy is a simple, efficient, and environmentally friendly pathway to prepare high performance cellulose films. The structure and morphology of multilayer tunicate cellulose films (MTCFs) were characterized by using FTIR and SEM measurements. The transparency and mechanical property of samples were investigated by UV-vis spectrophotometer and universal testing machine. Moreover, the biodegradation of multilayer films was also studied by soil burial method.

Experimental Section

Materials

Tunicate (*Ciona intestinalis*) was purchased from Weihai Evergreen Marine science and technology Co. Ltd (Shandong, China) and used as raw material. The microcrystalline cellulose was purchased from Shanghai Aladdin Biochemical Technology Co., Ltd (Shanghai, China) and used as a comparative sample. All other reagents were analytical grade purchased from Shanghai Chemical Agents Co. Ltd (Shanghai, China) and used without further purification.

Fabrication of multilayer films (MTCFs)

The tunics were obtained by removing the internal organs from tunicates (*Ciona intestinalis*) with a scalpel. The wet tunics were rinsed three times with deionized water, and immersed into NaOH solution (5 % w/v) at 80 °C for 3 hours (Zhao et al. 2018). After treatment, proteins, lipids and sediment were removed and and the films remained intact without dispersing into individual fiber. Finally, tunicate cellulose films were obtained by rinsing the films three times with deionized water.

Multilayer tunicate cellulose films (MTCFs) were prepared by layer-by-layer hot pressing of above tunicate cellulose films. A tunicate cellulose film was put between two Teflon films at 100 °C under a pressure of about 5 MPa for 1 hour to obtain single layer tunicate cellulose film (MTCF-1). Then MTCF-1 was wetted and superimposed with another tunicate cellulose film and repeated the above operation to obtain MTCF-

2. By analogy, a series of samples, including MTCF-4, MTCF-8, MTCF-10, and MTCF-12, were fabricated, respectively.

Characterization

Fourier transfer infrared spectroscopy (FTIR) was carried out using a NICOLET 5700 FTIR spectrometer (Thermo Fisher Scientific, USA). Scanning electron micrograph (SEM) measurements were taken with the field emission scanning electron microscopy (FESEM, Zeiss, Germany) at an accelerating voltage of 8 kV. The mechanical properties of multilayer tunicate cellulose films (MTCFs) were carried out using a universal material testing machine with a 1000 N load cell (Instron 5967, USA) at room temperature with a tensile speed of 5 mm min^{-1}. The optical transmittance of films was measured using Evolution 201 UV–vis spectrometer (Thermo Fisher Scientific, USA). Thermal gravimetric analysis was conducted using a Q500 (TA instrument, USA) under air at a heating rate of 10 °C/min from 80 to 600 °C. Wide-angle X-ray diffraction (WXRD) measurement was carried out on a XRD diffractometer (XPertPro, Panalytical, Netherlands). The crystallinity index (CrI) of the samples is caculated from the equation as follows: **see formula 1 in the supplementary files section.**

where I_{200} is the intensity of the (200) peak and I_{am} is the minimum intensity between the (110) and the (200) peak (French and Cintrón 2013; French 2014; French 2020; Ling et al. 2019).

Biodegradation Test

Multilayer films (5 × 4 cm^2) were buried about 20 cm beneath in natural soil. The average temperature and moisture of the soil were about 25 °C and 35%, respectively. The degraded samples were carefully taken out from soil each week, rinsed 3 times with deionized water, and dried at 25 °C for 2 days under vacuum before photograph. The weight loss of samples degraded in soil at one week intervals was measured for 12 weeks. SEM measurements of samples were conducted after degradation for 3 weeks.

Results And Discussion

Tunicate is well known as the only animal source of cellulose in the world and tunicate cellulose is superior to plant cellulose in terms of molecular weight and crystallinity (Wang et al. 2020). Therefore, tunicate cellulose nanocrystals with high aspect ratio and elastic modulus could be used as reinforcements to effectively improve the mechanical performance of polymeric materials (Zhang et al. 2017). Here, multilayer tunicate cellulose films were fabricated by a top-down approach, as shown in **Fig. 1**. First, tunic was separated from *Ciona intestijnali*s, and tunicate cellulose films were obtained by alkaline treatment to remove proteins, lipids, and sediment. Then, multilayer tunicate cellulose films were obtained by hot-pressing of tunicate cellulose films. To confirm the effectiveness of alkaline treatment, the FTIR spectra of pure cellulose, tunic before and after alkaline treatments are compared in **Fig. S1**. The characteristic peaks at 1240 cm^{-1} and 1540 cm^{-1} appeared in the spectrum of tunic which could be assigned to the C-O stretching of lipids and N-H stretching from amide groups of proteins, respectively. For tunicate cellulose film, only the typical peaks of cellulose could be observed, such as the absorption

peaks at 3420 cm^{-1} and 2900 cm^{-1} corresponded to -OH and C-H stretching, respectively; the peak at 1161 cm^{-1} and 1112 cm^{-1} were attributed to the C-O anti-symmetric bridge stretching and the C-OH skeletal vibration, respectively; the peaks at 1057 cm^{-1} and 1032 cm^{-1} were correspondence with the C-O-C pyranose ring skeletal vibration, and the small peak at 895 cm^{-1} originated from the glycosidic -CH deformation with a ring vibration and -OH bending, which was characteristic of β-glycosidic linkages between glucoses in cellulose (Nakashima et al. 2008). These results indicated that the lipids and proteins had been completely removed from tunic and tunicate cellulose film was successfully fabricated. After removal of protein and lipid, only tunicate cellulose was left in the form of nanofibers (**Fig. S2**).

The interaction between the film layers in the films was characterized by FTIR spectra. As shown in **Fig. S3**, large absorption bands at 3420 cm^{-1} were observed in the spectra of all samples, which could be attributed to -OH stretching. With the increase of layer number, these characteristic peaks become broader and stronger, revealing that strong hydrogen bonds formed between the layers during hot pressing process. The WXRD patterns and crystallinity index of tunic and tunicate cellulose film are shown in **Fig. S4**. Four main diffraction peaks located at 14.7, 16.5, 22.8 and 26.7^{o} could be observed in the WXRD patterns of tunic (**Fig. S4a**), reflecting the crystalline peaks of cellulose and the residual sand grain (Quero et al. 2018). For tunicate cellulose film, only three typical crystalline peaks at 14.7, 16.5, and 22.8^{o} were observed, corresponding to the (10), (110), and (200) crystal planes of cellulose I, respectively (Zhao and Li 2014). Moreover, upon applying the alkaline treatment, the crystallinity index increased from 55.6% for tunic to 85.0% for tunicate cellulose film, indicating that the lipids and proteins have been completely removed from tunic (**Fig. S4b**). These results were consistent with results of FTIR, revealing that only tunicate cellulose were retained after alkaline treatment.

Moreover, the morphologies of the cross section of multilayer tunicate films were investigated, as shown in **Fig. 2**. MTCF-1 exhibited uniform and compact morphology because slow evaporation of water during hot pressing caused the reassembly of tunicate cellulose nanofibers and the formation of dense structure (**Fig. 2a**). As the number of layers increased, no obvious boundary could be observed in the cross section of MTCF samples, indicating their good interfacial compatibility (**Fig. 2b-d**). However, MTCF-12 had the layered structure in the cross section, demonstrating that the reassembly of hydrogen bonds was limited by evaporating too much water during hot pressing (**Fig. 2e**). The thickness of samples linearly raised with the increase of the number of layers from 4.65 mm to 62.3 mm (**Fig. 2f**).

It is well known that the mechanical property of material was significantly dependence of its morphology. The tensile strength and toughness of multilayer tunicate cellulose films are shown in **Fig. 3**. The tensile strength and elongation at break of MTCF-1 were 41.8 MPa and 1.31 %, respectively, indicating its high stiffness and rigidity. Interestingly, both tensile strength and elongation at break of samples increased as the numbers of layers in the films. For MTCF-8, the tensile strength reached 140.3 MPa that was 3.4 times of MTCF-1, while the fracture strain was as high as 20.8 % that was also 3.4 times of MTCF-1 (**Fig. 3a**). The toughness of MTCF-8 was 13.2 MJ m^{-3}, which was the highest value of all samples. The improved

mechanical properties of films would benefit and widen their application in packaging field (Huang et al. 2020). However, the mechanical property of MTCF-12 was sharply decreased (**Fig. 3b**), which could be attributed to the defects in its layered structure. This results revealed that the layers with excellent interfacial compatibility could share the mechanical load, resulting in higher tensile strength. On the other hand, the sliding between the layers in the films benefited the improvement of their break at elongation, leading to their higher toughness (**Fig. S5**). These samples with good interfacial compatibility (from MTCF-1 to MTCF-8) showed flat fracture with tunicate cellulose nanofibers that had been pulled out, whereas MTCF-12 exhibited apparent defects in its fracture surface.

For packaging application, the optical property of film is also an important parameter. **Fig. 4a** displays the optical transmittance of MTCF samples from 400 to 800 nm. MTCF-1 had the highest transmittance, but the transparency of films decreased as the increase of the number of layers. The transmittance of MTCF samples descended from 83.6% to 62.8% at wavelength of 550 nm, when the number of layers increased from 1 to 12 (**Fig. 4b**). Light reflection and scattering occurred in the interfaces of films, resulting in the more layers had in the films the lower transparency was. Furthermore, the thermal stabilities of MTCFs were also studied and compared. **Fig. 4c** shows the thermogravimetric analysis (TGA) curves of MTCFs. Two steps of active weight loss of all samples could be observed with the elevating temperature. The main decomposition of all films into small molecules and condensable volatile macromolecules occurred from 200 to 350 °C. The second step at 350-500 °C could be assigned to the further decomposition of residues. After 500 °C, all samples were completely decomposed in air and reached constant weights. To investigate the temperature of maximum decomposition rates, DTG curves of samples are shown in **Fig. 4d**. For the first decomposition step, the T_{d1}values of all samples were 283, 295, 298, 300, and 301 °C for MTCF-1, MTCF-2, MTCF-4, MTCF-6, MTCF-8, respectively. This results demonstrated that the hydrogen bonding interaction between tunicate cellulose layers slightly enhanced the thermal stability of samples. The T_{d1} of MTCF-12 decreased to 298 °C could be attributed to the presence of defects in the film. In the second decomposition step, T_{d2} values of samples were 419, 429, 430, 438, and 442 °C, for MTCF-1, MTCF-2, MTCF-4, MTCF-6, MTCF-8, respectively, suggesting similar trend to the first stage. Due to its poor interfacial compatibility, MTCF-12 had a T_{d2} of 437 °C. These results indicated that strong hydrogen bonds between the tunicate cellulose layers improved their interfacial compatibility, resulting in good thermal stabilities of samples.

In the perspective of environmental protection, biodegradation of films is key factor for their application as packaging materials. **Fig. 5a** shows the photographs of various MTCFs after biodegradation in natural soil for different times. With the extension of degradation time, the size of the sample decreased gradually and finally disappeared completely. The biodegradation rate of samples depended on the number of tunicate cellulose layers in the films. For example, MTCF-1 completely degraded within 5 weeks but MTCF-12 needed 12 weeks (**Fig. 5b**). The weeks for complete degradation of various MTCF samples are shown in **Fig. 5c**. The complete degradation time are 5, 5, 7, 9, 11, and 12 weeks, for MTCF-1, MTCF-2, MTCF-4, MTCF-8, MTCF-10, and MTCF-12, respectively. When the samples had same area, it took longer time to degrade the thicker sample. To understand the degradation process, the SEM images

of samples after being buried in the soil for 3 weeks are shown in **Fig. 5d**. The porous morphology of samples indicated that microorganisms in the soil obtained nutrients by penetrating into the surface of MTCFs and directly decompose tunicate cellulose. These results indicated that all samples were biodegradable, which fulfilled the environmental concern as potential packaging materials.

Conclusion

We have successfully fabricated transparent and biodegradable multilayer films by hot pressing of tunicate cellulose film layers. This top-down approach efficiently promoted the formation of hydrogen bonds between two layers that was composed of tunicate cellulose nanofibers. The strong hydrogen bonding interactions offered good interfacial compatibility of materials, resulting in their improved thermal stabilities and excellent mechanical properties. Moreover, these resultant multilayer films could be completely degraded by microorganism in natural soil, and the biodegradation rate was dependence of the thickness of films. This work provided a top-down approach to manufacture degradable multilayer films from *Ciona intestijnali*s, which could be used as potential packaging materials instead of traditional plastics.

Declarations

ASSOCIATED CONTENT

Supporting Information. FTIR spectra of pure cellulose, tunicate cellulose film and tunic; SEM images of the tunicate cellulose film; FTIR spectra of MTCF-1, MTCF-2, MTCF-4, MTCF-6, MTCF-8 and MTCF-12; XRD patterns and crystallinity index of tunic and tunicate cellulose film; Mechanism diagram of toughness enhancement and SEM images for fracture surface of films.

AUTHOR INFORMATION

Corresponding Authors

Email: changcy@whu.edu.cn (C. Chang);

zhangqc1976@hubu.edu.cn (Q. Zhang)

ORCID: 0000-0002-3531-5964 (C. Chang)

Notes

The authors declare no competing financial interest.

Acknowledgements

This work was financially supported by the National Natural Science Foundation of China (52073217, 51873164), the National Key Research and Development Program of China (2018YFE0123700) and Key

Research and Development Program of Hubei Province (2020BCA079).

References

Barboza LGA, Vethaak AD, Lavorante B, Lundebye AK, Guilhermino L (2018) Marine microplastic debris: An emerging issue for food security, food safety and human health. Mar Pollut Bull 133:336-348. https://doi.org/10.1016/j.marpolbul.2018.05.047.

Cheng Q, Chang C, Zhang L (2016) Progress in tunicate cellulose based advanced functional materials. Sci Sin Chim 46:438-451. https://doi.org/10.1360/n032015-00265.

Cheng Q, Ye D, Chang C, Zhang L (2017) Facile fabrication of superhydrophilic membranes consisted of fibrous tunicate cellulose nanocrystals for highly efficient oil/water separation. J Membr Sci 525:1-8. https://doi.org/10.1016/j.memsci.2016.11.084.

Cheng Q, Ye D, Yang W, Zhang S, Chen H, Chang C, Zhang L (2018) Construction of Transparent Cellulose-Based Nanocomposite Papers and Potential Application in Flexible Solar Cells. ACS Sustainable Chem Eng 6:8040-8047. https://doi.org/10.1021/acssuschemeng.8b01599.

French AD, Santiago Cintrón M (2013) Cellulose polymorphy, crystallite size, and the Segal crystallinity index. Cellulose 20: 583-588. https://doi.org/10.1007/s10570-012-9833-y.

French AD (2014) Idealized powder diffraction patterns for cellulose polymorphs. Cellulose 21:885-896. https://doi.org/10.1007/s10570-013-0030-4.

French AD (2020) Increment in evolution of cellulose crystallinity analysis. Cellulose 27:5445-5448. https://doi.org/10.1007/s10570-020-03172-z.

Gao X, Huang L, Wang B, Xu D, Zhong J, Hu Z, Zhang L, Zhou J (2016) Natural Materials Assembled, Biodegradable, and Transparent Paper-Based Electret Nanogenerator. ACS Appl Mater Interfaces 8:35587-35592. https://doi.org/10.1021/acsami.6b12913.

Geyer R, Jambeck JR, Law KL (2017) Production, use, and fate of all plastics ever made. Sci Adv, 3:e1700782. https://doi.org/10.1126/sciadv.1700782.

Hu W, Fang Z, Liu Y, Zhou Y, Kuang Y, Ning H, Li B, Chen G, Liu Y (2018) Protonation Process to Enhance the Water Resistance of Transparent and Hazy Paper. Acs Sustainable Chem Eng 6:12385-12392. https://doi.org/10.1021/acssuschemeng.8b02900.

Huang S, Liu X, Chang C, Wang Y (2020) Recent developments and prospective food-related applications of cellulose nanocrystals: a review. Cellulose 27:2991-3011. https://doi.org/10.1007/s10570-020-02984-3.

Jia C, Li T, Chen CJ, Dai J, Kierzewski I, Song J, Li Y, Yang C, Wang C, Hu L (2017) Scalable, anisotropic transparent paper directly from wood for light management in solar cells. Nano Energy 36:366-373. https://doi.org/10.1016/j.nanoen.2017.04.059.

Jiang F, Li T, Li Y, Zhang Y, Gong A, Dai J, Hitz E, Hu L (2018) Wood-Based Nanotechnologies toward Sustainability. Adv Mater 30:e1703453. https://doi.org/10.1002/adma.201703453.

Jung Y, Chang T, Zhang H, Yao C, Zheng Q, Yang V, Mi H, Kim M, Cho S, Park D, Jiang H, Lee J, Qiu Y, Zhou W, Cai Z, Gong S, Ma Z (2015) High-performance green flexible electronics based on biodegradable cellulose nanofibril paper. Nat Commun 6:7170. https://doi.org/10.1038/ncomms8170.

Keplinger T, Wittel FK, Ruggeberg M, Burgert I (2020) Wood Derived Cellulose Scaffolds-Processing and Mechanics. Adv Mater e2001375. https://doi.org/10.1002/adma.202001375.

Klemm D, Heublein B, Fink HP, Bohn A (2005) Cellulose: fascinating biopolymer and sustainable raw material. Angew Chem Int Ed Engl 44:3358-3393. https://doi.org/10.1002/anie.200460587.

Koppolu R, Lahti J, Abitbol T, Swerin A, Kuusipalo J, Toivakka M (2019) Continuous Processing of Nanocellulose and Polylactic Acid into Multilayer Barrier Coatings. ACS Appl Mater Interfaces 11:11920-11927. https://doi.org/10.1021/acsami.9b00922.

Li T, Zhu M, Yang Z, Song J, Dai J, Yao Y, Luo W, Pastel G, Yang B, Hu L (2016) Wood Composite as an Energy Efficient Building Material: Guided Sunlight Transmittance and Effective Thermal Insulation. Adv Energy Mater 6:e1601122. https://doi.org/10.1002/aenm.201601122.

Li T, Song J, Zhao X, Yang Z, Pastel G, Xu S, Jia C, Dai J, Chen C, Gong A, Jiang F, Yao Y, Fan T, Yang B, Wagberg L, Yang R, Hu L (2018) Anisotropic, lightweight, strong, and super thermally insulating nanowood with naturally aligned nanocellulose. Sci Adv 4:eaar3724. https://doi.org/10.1126/sciadv.aar3724.

Li T, Zhai Y, He S, Gan W, Wei Z, Heidarinejad M, Dalgo D, Mi R, Zhao X, Song J, Dai J, Chen C, Ailli A, Vellore A, Martini A, Yang R, Srebric J, Yin X, Hu L (2019) A radiative cooling structural material. Science 364:760-763. https://doi.org/10.1126/science.aau9101.

Ling Z, Wang T, Makarem M, Santiago Cintrón M, Cheng HN, Kang X, Bacher M, Potthast A, Rosenau T, King H, Delhom CD, Nam S, Edwards JV, Kim SH, Xu F, French AD (2019) Effects of ball milling on the structure of cotton cellulose. Cellulose 26:305-328. https://doi.org/10.1007/s10570-018-02230-x.

Mohanty A, Vivekanandhan S, Pin J, Misra M (2018) Composites from renewable and sustainable resources: Challenges and innovations. Science 362:536-542. https://doi.org/10.1126/science.aat9072.

Nakashima K, Sugiyama J, Satoh N (2008) A spectroscopic assessment of cellulose and the molecular mechanisms of cellulose biosynthesis in the ascidian Ciona intestinalis. Mar Genom 1:9-14. https://doi.org/10.1016/j.margen.2008.01.001.

Peng N, Huang D, Gong C, Wang Y, Zhou J, Chang C (2020) Controlled Arrangement of Nanocellulose in Polymeric Matrix: From Reinforcement to Functionality. ACS Nano 14:16169-16179. https://doi.org/10.1021/acsnano.0c08906.

Quero F, Opazo G, Zhao Y, Feschotte-Parazon A, Fernandez J, Quintro A, Flores M (2018) Top-down Approach to Produce Protein Functionalized and Highly Thermally Stable Cellulose Fibrils. Biomacromolecules 19:3549-3559. https://doi.org/10.1021/acs.biomac.8b00831.

Siracusa V, Rocculi P, Romani S, Rosa MD (2008) Biodegradable polymers for food packaging: a review. Trends Food Sci Tech 19:634-643. https://doi.org/10.1016/j.tifs.2008.07.003.

Wang J, Li X, Cheng Q, Lv F, Chang C, Zhang L (2020) Construction of beta-FeOOH@tunicate cellulose nanocomposite hydrogels and their highly efficient photocatalytic properties. Carbohyd Polym 229:115470. https://doi.org/10.1016/j.carbpol.2019.115470.

Wang S, Jiang F, Xu X, Kuang Y, Fu K, Hitz E, Hu L (2017) Super-Strong, Super-Stiff Macrofibers with Aligned, Long Bacterial Cellulose Nanofibers. Adv Mater 29:e1702498. https://doi.org/10.1002/adma.201702498.

Wang S, Li T, Chen C, Kong W, Zhu S, Dai J, Diaz A, Hitz E, Solares S, Hu L (2018) Transparent, Anisotropic Biofilm with Aligned Bacterial Cellulose Nanofibers. Adv Funct Mater 28:e1707491. https://doi.org/10.1002/adfm.201707491.

Ye D, Lei X, Li T, Cheng Q, Chang C, Hu L, Zhang L (2019) Ultrahigh Tough, Super Clear, and Highly Anisotropic Nanofiber-Structured Regenerated Cellulose Films. ACS Nano 13:4843-4853. https://doi.org/10.1021/acsnano.9b02081.

Zhan H, Peng N, Lei X, Huang Y, Li D, Tao R, Chang C (2018) UV-induced self-cleanable TiO2/nanocellulose membrane for selective separation of oil/water emulsion. Carbohyd Polym 201:464-470. https://doi.org/10.1016/j.carbpol.2018.08.093.

Zhan H, Zuo T, Tao R, Chang C (2018) Robust Tunicate Cellulose Nanocrystal/Palygorskite Nanorod Membranes for Multifunctional Oil/Water Emulsion Separation. ACS Sustainable Chem Eng 6:10833-10840. https://doi.org/10.1021/acssuschemeng.8b02137.

Zhang T, Zuo T, Hu D, Chang C (2017) Dual Physically Cross-Linked Nanocomposite Hydrogels Reinforced by Tunicate Cellulose Nanocrystals with High Toughness and Good Self-Recoverability. ACS Appl Mater Interfaces 9:24230-24237. https://doi.org/10.1021/acsami.7b06219.

Zhao Y, Li J (2014) Excellent chemical and material cellulose from tunicates: diversity in cellulose production yield and chemical and morphological structures from different tunicate species. Cellulose 21:3427-3441. https://doi.org/10.1007/s10570-014-0348-6.

Zhao Y, Moser C, Henriksson G (2018) Transparent Composites Made from Tunicate Cellulose Membranes and Environmentally Friendly Polyester. ChemSusChem 11:1728-1735. https://doi.org/10.1002/cssc.201800627.

Zhu H, Luo W, Ciesielski PN, Fang Z, Zhu JY, Henriksson G, Himmel M, Hu L (2016a) Wood-Derived Materials for Green Electronics, Biological Devices, and Energy Applications. Chem Rev 116:9305-9374. https://doi.org/10.1021/acs.chemrev.6b00225.

Zhu M, Li T, Davis C, Yao Y, Dai J, Wang Y, AlQatari F, Gilman J, Hu L (2016b) Transparent and haze wood composites for highly efficient broadband light management in solar cells. Nano Energy 26:332-339. https://doi.org/10.1016/j.nanoen.2016.05.020.

Zhu M, Wang Y, Zhu S, Xu L, Jia C, Dai J, Song J, Yao Y, Wang Y, Li Y, Henderson D, Luo, W, Li H, Minus M, Li T, Hu L (2017) Anisotropic, Transparent Films with Aligned Cellulose Nanofibers. Adv Mater 29:e1606284. https://doi.org/10.1002/adma.201606284.

Zhu M, Jia C, Wang Y, Fang Z, Dai J, Xu L, Huang D, Wu J, Li Y, Song J, Yao Y, Hitz E, Wang Y, Hu L (2018) Isotropic Paper Directly from Anisotropic Wood: Top-Down Green Transparent Substrate Toward Biodegradable Electronics. ACS Appl Mater Interfaces 10:28566-28571. https://doi.org/10.1021/acsami.8b08055.

Figures

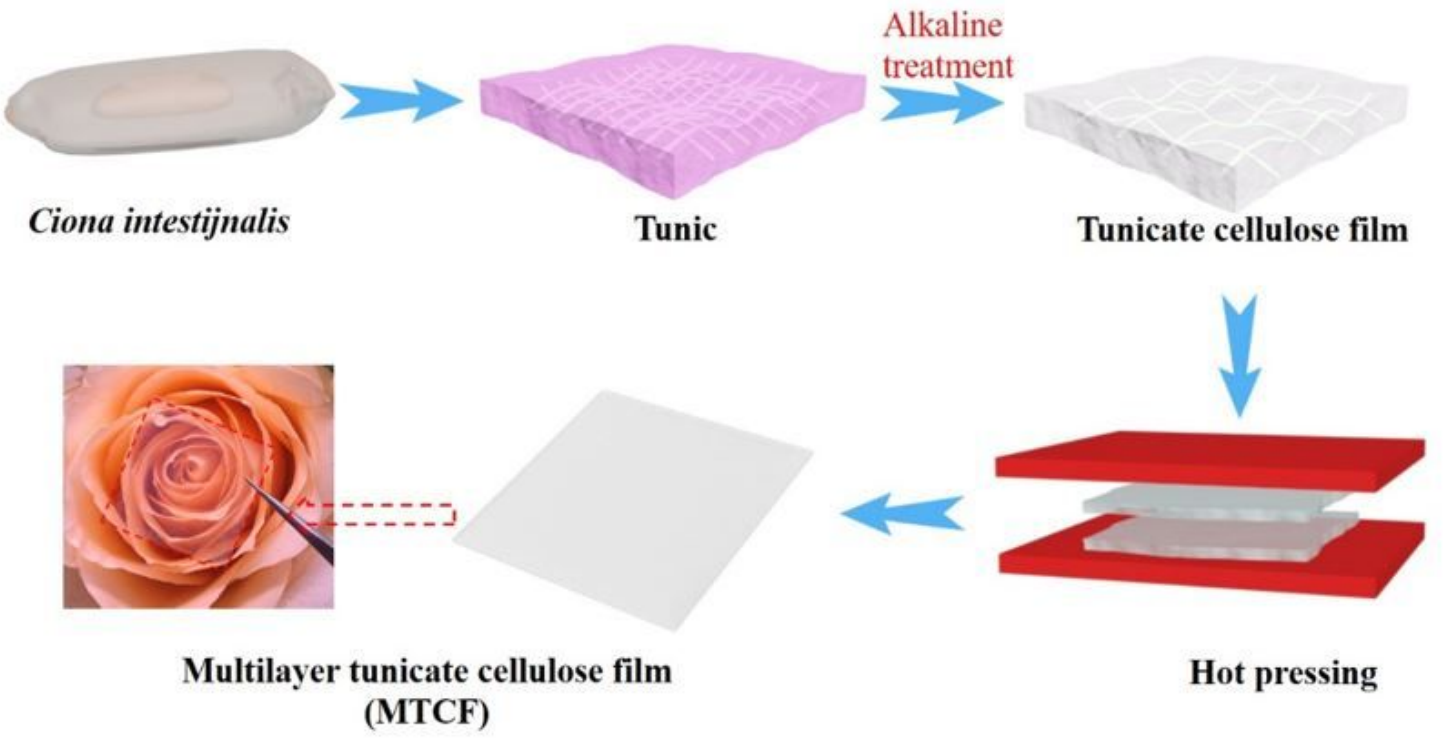

Figure 1

Schematic illustration for preparation of multilayer tunicate cellulose films (MTCFs).

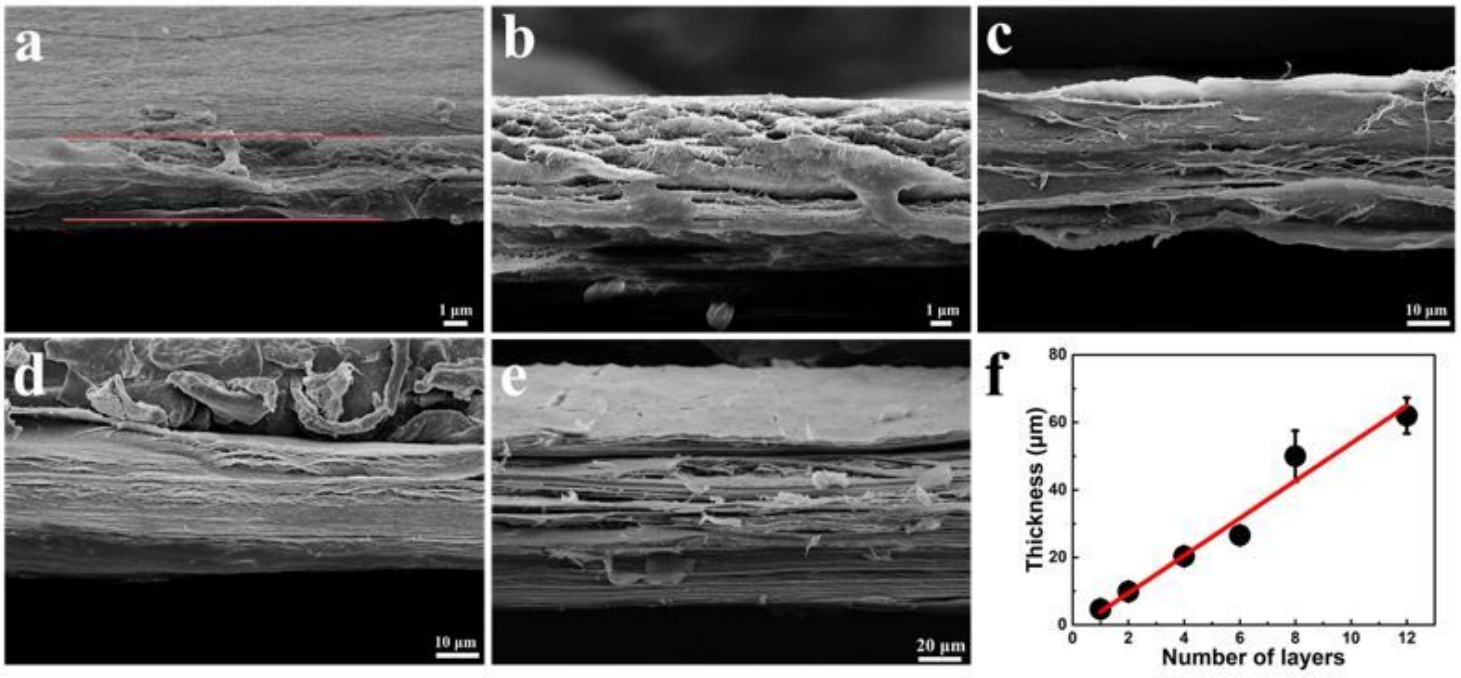

Figure 2

SEM images for cross section of multilayer tunicate cellulose films: MTCF-1 (a), MTCF-2 (b), MTCF-4 (c), MTCF-6 (d) and MTCF-12 (e). (f) Thickness versus layer number curve of the multilayer tunicate cellulose films (MTCFs).

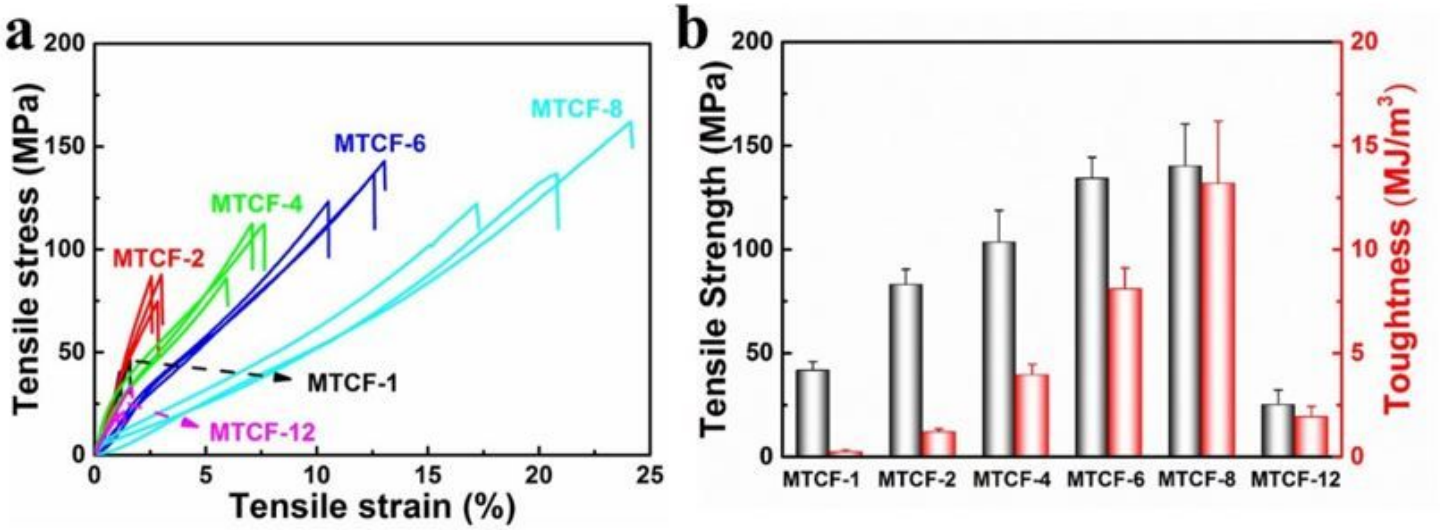

Figure 3

Mechanical properties of multilayer tunicate cellulose films: (a) tensile stress–strain curves and (b) comparison of tensile strength and toughness.

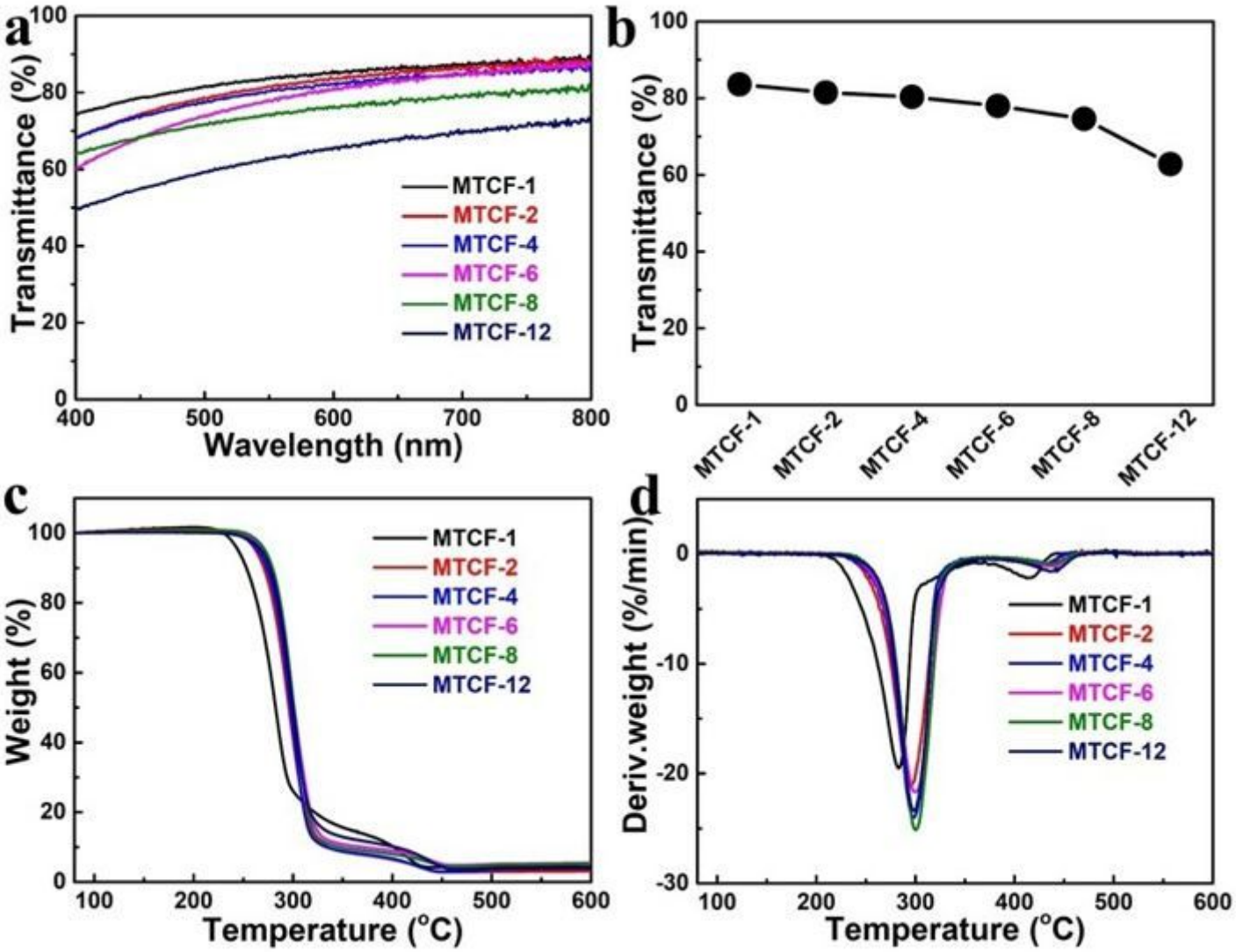

Figure 4

Broadband transmittance (a) and transmittance versus layer number curve of MTCFs at 550 nm (b). Thermogravimetric analysis curves (c) and their corresponding first derivative thermogravimetric curves (d) of MTCFs.

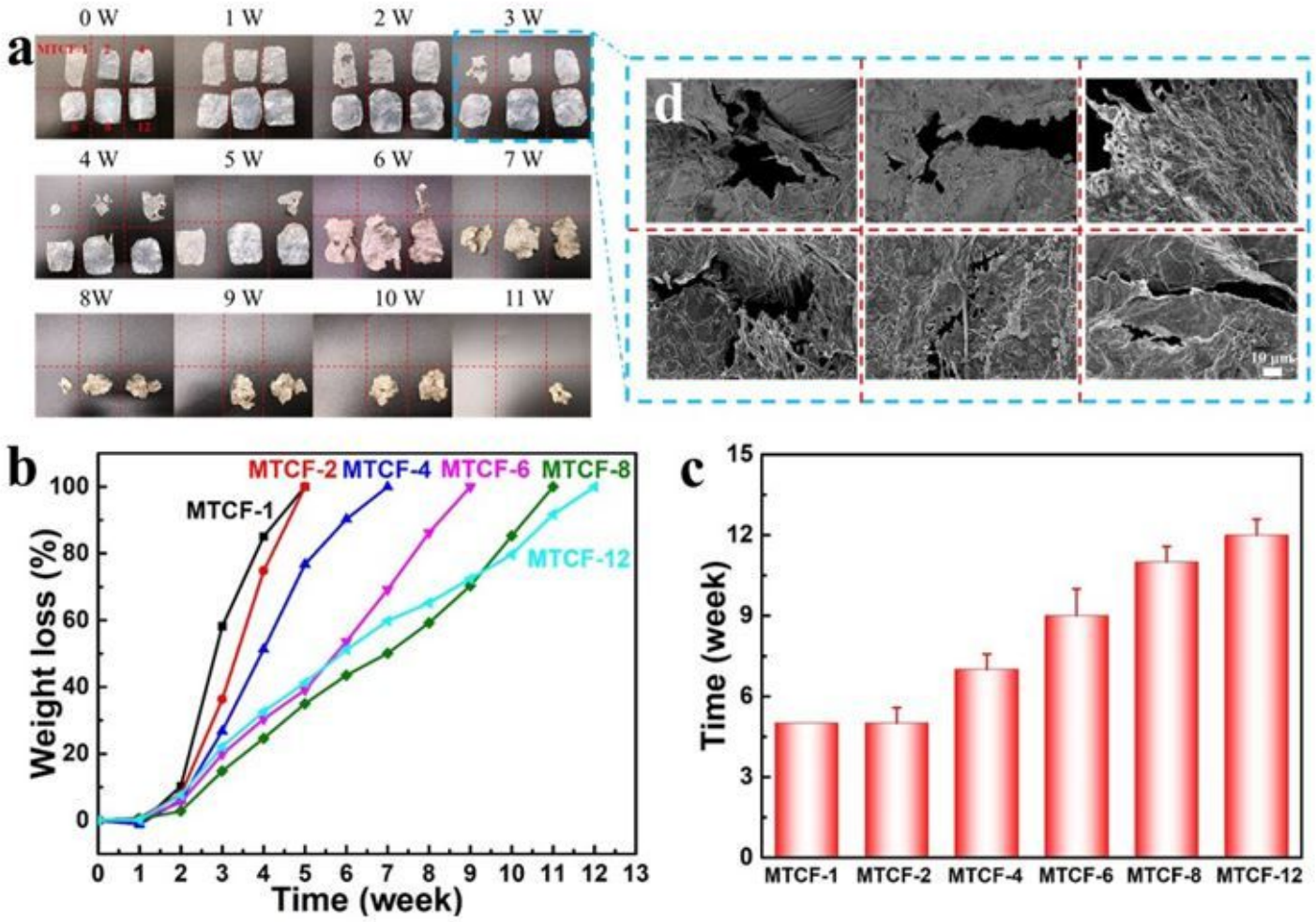

Figure 5

Biodegradation of MTCFs: (a) digital pictures, (b) weight loss vs. degradation time, (c) time for complete degradation, and (d) SEM images for the surface of MTCF samples from MTCF-1 to MTCF-12 after degrading for 3 weeks.

Supplementary Files

This is a list of supplementary files associated with this preprint. Click to download.

- Supportinginformation.docx
- formula.docx